Research Article

Jiaqi Wang*, Lulu Zhang, Tingting Cao, Haiou Zhang, Yingying Sun, Yingguo Wang, Chenxi Yang, Yantao Hu

Investigating the adsorption mechanism of zinc chloride-modified porous carbon for sulfadiazine removal from water

https://doi.org/10.1515/chem-2024-0065
received March 17, 2024; accepted June 24, 2024

Abstract: Sulfadiazine (SDZ) is a commonly used antibiotic in medicine, aquaculture, and animal husbandry. However, its misuse has resulted in its release into soil and water environments, posing a gradual threat to the environment and human health. In this study, cotton pulp, poplar sawdust, and corn stover were chosen as raw materials. Zinc chloride ($ZnCl_2$) was used as a modifier to prepare modified porous carbon through pyrolysis at different carbonization temperatures (400 and 800°C). The objective was to investigate the adsorption effect and mechanism of modified porous carbon on SDZ in aqueous environments, as well as the effect of different biomass fractions of the carbon source on the adsorption effect. The physical and chemical properties of the modified porous carbon were characterized by various means of characterization, and the results showed that the high temperature and modification effects made the adsorbent material possess a larger specific surface area and richer pore structure, higher aromaticity, higher degree of graphitization, etc., which would be beneficial for the adsorption of SDZ. Among them, CCPZ800 showed the highest saturation adsorption of SDZ, Q_{max} = 425.45 mg/g. The adsorption experiments were carried out by changing the initial conditions and fitted with kinetic and isothermal adsorption to further explain the adsorption mechanism of modified porous carbon on SDZ in conjunction with the adsorption of SDZ by hydrothermal carbon materials. The results showed that the adsorption of modified porous carbon on SDZ conformed to the quasi-secondary kinetic and Freundlich isothermal adsorption models. Adsorption mechanism of SDZ on modified porous carbon followed a multimolecular layer adsorption, with chemical adsorption being the dominant process. Both physical adsorption and chemical adsorption occurred simultaneously, with the main adsorption mechanism being π–π conjugation. In addition, compositional distribution of biomass from different carbon sources results in variations in pyrolysis mode and pyrolysis products, which in turn affect adsorption. By analyzing the effect of variability in the composition of biomass on the adsorption effect of SDZ, it can be concluded that higher cellulose content in the carbon source leads to a better adsorption effect of SDZ. The study showcases the effectiveness of $ZnCl_2$-modified porous carbon in removing SDZ from water, offering insights into the selection of raw materials for this adsorbent preparation.

Keywords: sulfadiazine, modified porous carbon, zinc chloride, biomass, adsorption mechanism, water contamination

*** Corresponding author: Jiaqi Wang,** Shaanxi Provincial Land Engineering Construction Group Co., Ltd, Xi'an, 710075, China; Institute of Land Engineering and Technology, Shaanxi Provincial Land Engineering Construction Group Co., Ltd, Xi'an, 710075, China; Key Laboratory of Degraded and Unused Land Consolidation Engineering, Ministry of Natural Resources, Xi'an, 710075, China, e-mail: 707605048@qq.com

Lulu Zhang, Chenxi Yang: Shaanxi Provincial Land Engineering Construction Group Co., Ltd, Xi'an, 710075, China; Shaanxi Engineering Research Center of Land Consolidation, Xi'an, 710075, China; Land Engineering Technology Innovation Center, Ministry of Natural Resources, Xi'an, 710075, China

Tingting Cao, Yingying Sun: Shaanxi Provincial Land Engineering Construction Group Co., Ltd, Xi'an, 710075, China; Land Engineering Technology Innovation Center, Ministry of Natural Resources, Xi'an, 710075, China

Haiou Zhang: Shaanxi Provincial Land Engineering Construction Group Co., Ltd, Xi'an, 710075, China; Institute of Land Engineering and Technology, Shaanxi Provincial Land Engineering Construction Group Co., Ltd, Xi'an, 710075, China; Land Engineering Technology Innovation Center, Ministry of Natural Resources, Xi'an, 710075, China

Yingguo Wang: Shaanxi Provincial Land Engineering Construction Group Co., Ltd, Xi'an, 710075, China; Institute of Land Engineering and Technology, Shaanxi Provincial Land Engineering Construction Group Co., Ltd, Xi'an, 710075, China

Yantao Hu: Shaanxi Provincial Land Engineering Construction Group Co., Ltd, Xi'an, 710075, China

1 Introduction

Sulfonamide antibiotics (SAs) have a long history of use as synthetic antibiotics and are widely consumed in China [1]. Among them, sulfadiazine (SDZ) is commonly used in agriculture and farming as an effective anti-infective drug [2]. However, studies have indicated that SDZ is resistant to degradation and can easily migrate, leading to its accumulation in soil and water bodies [3]. This accumulation poses a significant risk to the ecological environment [4]. Additionally, SDZ can be transferred through the food chain and accumulate in humans, thereby posing a threat to human health [5,6].

For the remediation of SA pollution, various methods are commonly employed, including biodegradation, chemical oxidation, and adsorption [7]. Among these methods, adsorption stands out due to its ease of operation and lower potential for causing secondary pollution [8]. Biochar, a carbon material obtained through high-temperature cracking of waste biomass, is frequently used as an adsorption material due to its affordability and simple preparation process [9]. However, the effectiveness of traditional biochar in adsorption is often unsatisfactory due to factors such as limited pore space, fewer functional groups, and low degree of aromatization [10]. To enhance the adsorption performance of biochar, researchers often employ acid–base modification and metal salt impregnation [11]. These modifications lead to the development of porous carbon with increased pore space, larger specific surface area, more functional groups, and higher aromaticity. Among many modifiers, zinc chloride ($ZnCl_2$) is one of the most effective modifiers for the preparation of porous carbon materials [12], which accelerates the dissolution of cellulose (CE), hemicellulose (HE), and lignin (LI) in biomass constituents, resulting in the formation of a three-dimensional and interconnected porous structure. Some researchers prepared $ZnCl_2$-modified porous carbon materials from coffee grounds, and the results showed that $ZnCl_2$ modification could significantly enhance the adsorption of methylene blue by the adsorbent [13]. $ZnCl_2$ modification can keep more carbon immobilized and increase the specific surface area and porosity of the material, which in turn enhances the adsorption capacity of the material and the ability to adsorb pollutants [14]. Additionally, $ZnCl_2$ disrupts the graphitic structure of biomass-derived carbon, enhancing the degree of graphitization of the biochar [15]. Moreover, zinc serves as a backbone during the carbonization process, improving the degree of carbonization and aromaticity of the biochar [16].

The use of modified porous carbon in the treatment of antibiotic contamination is currently widespread [17]. Porous carbon interacts with pollutants through various adsorption methods, including pore adsorption, electrostatic attraction, π–π conjugation, and hydrogen bonding [18]. The adsorption of porous carbon materials varies significantly depending on the raw materials and methods used for their preparation [19,20]. Therefore, in this study, we utilized cotton pulp, corn stover (CS), and poplar sawdust (PS) as biomass with distinct compositions. Zinc chloride was employed as a modifier to prepare the modified porous carbon at different cracking temperatures. The physicochemical properties and structural differences of the porous carbon were analyzed under different conditions using structural characterization techniques. Additionally, adsorption experiments were conducted using SDZ as a pollutant to elucidate the adsorption mechanism of the porous carbon on SDZ. These experiments aimed to further understand the adsorption behavior of SDZ on porous carbon and analyze the impact of the distribution of biomass components on the adsorption effect. The results of this study will help to deepen the understanding of the adsorption behavior of SDZ in the aqueous environment and provide assistance in the preparation of the initial carbon source selection for the adsorbent materials for the removal of SAs in the aqueous environment, which will help to solve the status quo of SDZ antibiotic pollution, and is of practical significance in the management of antibiotic pollution in the aqueous environment and the sustainable development of the environment.

2 Materials and methods

2.1 Preparation of carbon materials

The raw material cotton pulp (CP) was taken from a university light industry institute, and PS and CS were taken from the park and farmland. The raw materials were cleaned, naturally dried, and then transferred to the oven at 65°C for 2 h, and then crushed and sieved. The raw materials of modified porous carbon should be weighed and mixed with a saturated solution of $ZnCl_2$ according to a certain proportion, then impregnated for 24 h, and then used.

In the experiment, the unmodified carbon materials and modified porous carbon were prepared by the oxygen-limited cracking method, the raw materials were spread into the quartz boat and put into the tube furnace, and the protective gas nitrogen was introduced to make the furnace chamber in an adiabatic state, and the temperature of the furnace chamber was raised to the target temperature (400 or 800°C) and held for 2 h at the rate of 10°C/min after the gas was stabilized, the pyrolysis was finished, and the products were

washed by boiling with 1 mol/L hydrochloric acid, and washed to neutral with pure water, transferred to the oven at 90°C for drying, and then ground and bagged for spare use. At the end of pyrolysis, the pyrolysis product was washed with 1 mol/L hydrochloric acid to remove impurities by heating and boiling, washed to neutrality with pure water, transferred to an oven at 90°C for drying, and then ground and bagged for spare use, and labeled according to the raw material, temperature, and modifier as CCP400/800, CPS400/800, CCS400/800, CCPZ400/800, CPSZ400/800, and CCSZ400/800 (CP, PS, CS is the raw material type, Z is $ZnCl_2$ modified, and 400, 800 represents the temperature).

The hydrothermal carbon spheres were prepared by the hydrothermal synthesis method. The raw materials were put into a high-pressure reactor, added 50 mL of pure water, and fully reacted at a temperature of 260°C for 8 h. At the end of the reaction, it was cooled down to room temperature and taken out, and then soaked in ethanol and repeatedly centrifuged to clean for more than three times, and then cleaned until the liquid was colorless and then put into the oven at 90°C to be used for drying, labeled with HCCP, HCPS, and HCCS (CP, PS, and CS represent the raw material types, respectively, and HC is the hydrothermal carbon).

2.2 Characterization of carbon materials

The physical and chemical properties and characteristics of the carbon materials were examined using scanning electron microscopy (SEM), Fourier transform infrared spectroscopy (FTIR), Brunauer, Emmett and Teller, X-ray diffraction (XRD), and X-ray photoelectron spectroscopy (XPS). An SEM (Tescan, Czech Republic) was used to observe the micro-morphology and characteristics of the carbon materials. A fully automatic specific surface area analyzer (Quantachrome, USA) was used to analyze the specific surface area and other pore structure parameters of the carbon materials. The FTIR functional group analysis of the carbon materials was carried out at 500–4,000 cm^{-1} by FTIR spectrometer (Bruker, Germany), and the solid-phase composition of the carbon materials was analyzed by X-ray diffractometer (Bruker, Germany) at a 2θ angle of 10°–70°. X-ray photoelectron spectrometry (Thermo Fisher, USA) was used to radiate the samples with an Alkα X-ray source, with a spot size of 400°–70°. X-ray photoelectron spectrometer (Thermo Fisher, USA) was used to analyze the elemental and structural compositions of the carbon materials using an Alkα X-ray source with a spot size of 400 μm, a fluence energy of 150 eV, and a binding energy range of 1,350–0 eV.

2.3 Carbon material adsorption experiments

The target pollutant SDZ (Aladdin, USA, purity ≥98%) was prepared as a stock solution using deionized water. The modified porous carbon with better adsorption effect on SDZ was preferred, and the effects of adsorbent addition (1–100 mg), pH (2–12), adsorption time (1–2,880 min), and the initial concentration of pollutants (1–50 mg/L) on the adsorption amount of SDZ were investigated, and adsorption kinetics and isothermal adsorption were fitted to analyze the adsorption mechanism.

Batch adsorption experiments were conducted on SDZ using hydrothermal carbon materials prepared from different carbon sources as well as modified porous carbon materials prepared from three components of biomass: CE, HE, and LI (Aladdin, USA), respectively, to further explain the adsorption mechanism and the effect of the differences in the composition of the feedstocks on the adsorption amount.

2.4 Adsorption, kinetics, isothermal equations

The adsorbent adsorption capacity is calculated as

$$Q_e = \frac{(C_0 - C_e) \times V}{m},$$

where Q_e is the amount of SDZ adsorbed by the porous carbon (mg/g), C_0 represents the initial concentration of SDZ (mg/L), C_e denotes the concentration of SDZ after the end of adsorption (mg/L), V represents the volume of the solution (L), and m represents the amount of absorbent added (g).

The adsorption kinetics were fitted to the adsorption process using quasi-primary kinetics, and quasi-secondary kinetics. The quasi-primary adsorption kinetics was modeled as

$$\ln(Q_e - Q_t) = \ln Q_e - k_1 t,$$

where Q_e (mg/g) is the equilibrium adsorption amount at the adsorption equilibrium of the modified porous carbon, Q_t (mg/g) is the adsorption amount at the moment t, and k_1 is the quasi-secondary adsorption kinetic constant. The quasi-secondary adsorption kinetic modeling equation is

$$\frac{t}{Q_t} = \frac{1}{k_2 Q_e^2} + \frac{t}{Q_e},$$

where Q_e (mg/g) is the equilibrium adsorption of SDZ on porous carbon at adsorption equilibrium, Q_t (mg/g) is the

adsorption of SDZ at time t, and k_2 is the kinetic constant of quasi-secondary adsorption.

Langmuir isothermal adsorption model and Freundlich isothermal adsorption model were selected for isothermal fitting of the adsorption process of the adsorbent. Langmuir isothermal adsorption model equations are given below:

$$\frac{C_e}{Q_e} = \frac{C_e}{Q_{max}} + \frac{1}{Q_{max}K_L},$$

where Q_{max} is the saturated adsorption of SDZ at adsorption equilibrium (mg/g), Q_e is the amount of SDZ adsorbed at different concentrations (mg/g), and C_e is the concentration of SDZ (mg/L). K_L is the Langmuir's constant.

The Freundlich isothermal adsorption model equation is given below:

$$\ln Q_e = \ln K_F + \frac{1}{n}\ln C_e,$$

where Q_e is the amount of SDZ adsorbed at different concentrations (mg/g), C_e is the concentration of SDZ (mg/L) while KF and n are Freundlich adsorption constants.

2.5 Analysis methods

SDZ was detected using liquid chromatography, and the supernatant after adsorption was filtered through 0.22 μm filter membrane and loaded into liquid chromatography vials for determination using HPLC1290 high performance liquid chromatograph (HPLC, 1290, Agilent, USA).

Chromatographic conditions: Column: EclipsePlusC18 (2.1 × 100 mm); Detection wavelength: 280 μm; Injection volume: 20 μL; Mobility V (C_2H_3N):V (0.01 mol/L H_3PO_4) = 20:80.

3 Results

3.1 Characterization of the morphology and pore structure of carbon materials

High temperatures and modifications cause significant changes in the microstructure of the carbon material. However, the unmodified materials still retain some of their original structure, such as the fibrous structure of CP and the lamellar structure of PS. The appearance of the $ZnCl_2$-modified porous carbon materials undergoes significant changes, with visible pore structures (Figure 1). This is mainly attributed to the catalytic dehydration of the raw material by $ZnCl_2$. As the temperature increases, the modification process becomes more intense, leading to the destruction, polymerization, and deformation of the original biomass structure. This results in the release of H and O, and the overflow of water vapor, ultimately forming a porous structure [15].

The modified carbon materials exhibited a significant increase in specific surface area and pore volume, with the carbonization temperature playing a crucial role in enhancing these properties (Table 1). CCPZ800 showed the highest total specific surface area of 1663.62 m^2/g and pore volume of

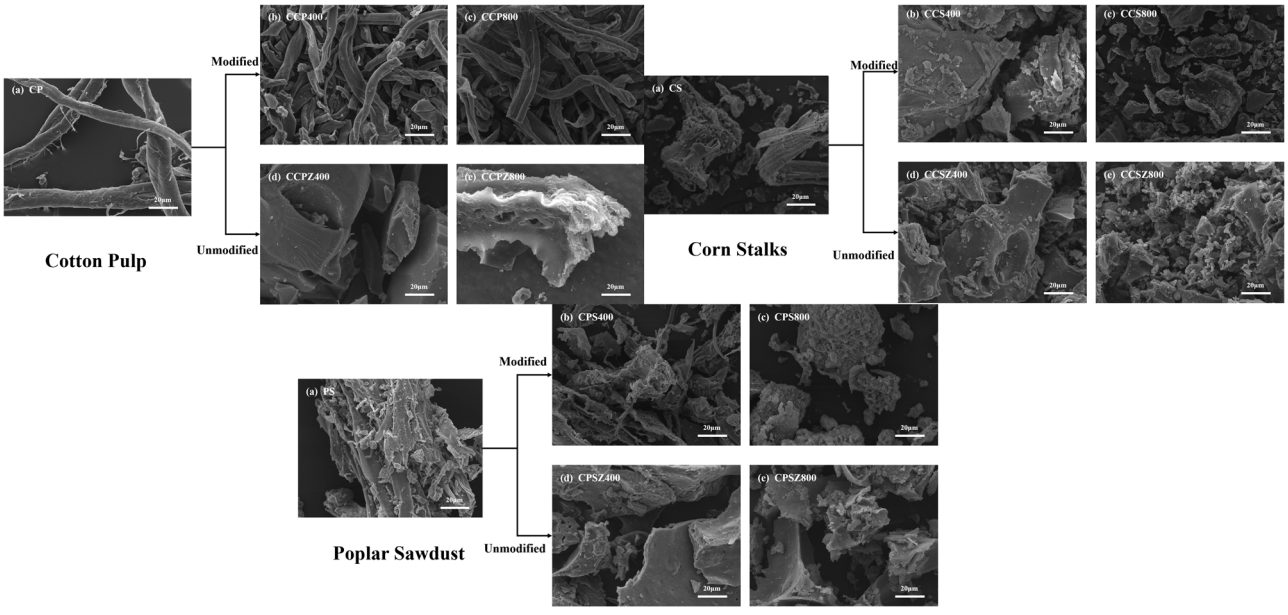

Figure 1: SEM images of carbon materials prepared from three biomasses.

Table 1: Pore structure parameters of raw materials and carbon materials

Material	Specific surface area (m^2/g)	Mesoporous specific surface area (m^2/g)	Microporous specific surface area (m^2/g)	Total pore volume (cm^3/g)	Mesopore pore volume (cm^3/g)	Microporous pore volume (cm^3/g)	Average pore diameter (nm)
CP	40.67	8.62	0	0.002	0.002	0	8.14
CCP400	85.25	11.25	0	0.012	0.008	0	7.64
CCP800	110.27	75.26	0	0.027	0.008	0	6.95
CCPZ400	935.02	53.12	803.65	0.547	0.071	0.334	2.33
CCPZ800	1663.62	685.19	62.08	1.255	0.668	0.007	3.02
PS	56.47	5.16	0	0.001	0.001	0	8.34
CPS400	68.54	9.15	0	0.009	0.003	0	7.62
CPS800	91.25	52.64	0	0.021	0.015	0	7.18
CPSZ400	352.66	66.82	116.77	0.262	0.119	0.069	2.98
CPSZ800	669.26	332.65	101.64	0.764	0.555	0.039	4.56
CS	43.17	2.62	0	0.001	0.001	0	7.14
CCS400	62.16	21.62	0	0.013	0.005	0	6.95
CCS800	105.15	68.25	0	0.029	0.016	0	6.44
CCSZ400	589.38	137.30	161.77	0.445	0.197	0.146	3.02
CCSZ800	741.03	496.66	26.28	0.803	0.640	0.005	4.33

1.255 cm^3/g. The adsorption/de-adsorption curves of $ZnCl_2$-modified porous carbon exhibited consistent Type IV adsorption isotherm characteristics (Figure 2) with hysteresis loops. The modified porous carbon prepared at a low carbonization temperature of 400°C (Figure 2a–c) displayed H4-type hysteresis loops, primarily attributed to microporous structures. On the other hand, the modified porous carbon prepared at a high carbonization temperature of 800°C (Figure 2d–f) exhibited H2-type hysteresis loops, mainly due to the presence of mesoporous structures. This transition was likely caused by the melting and collapsing of the microporous structures, leading to the formation of mesopores as the temperature increased [21].

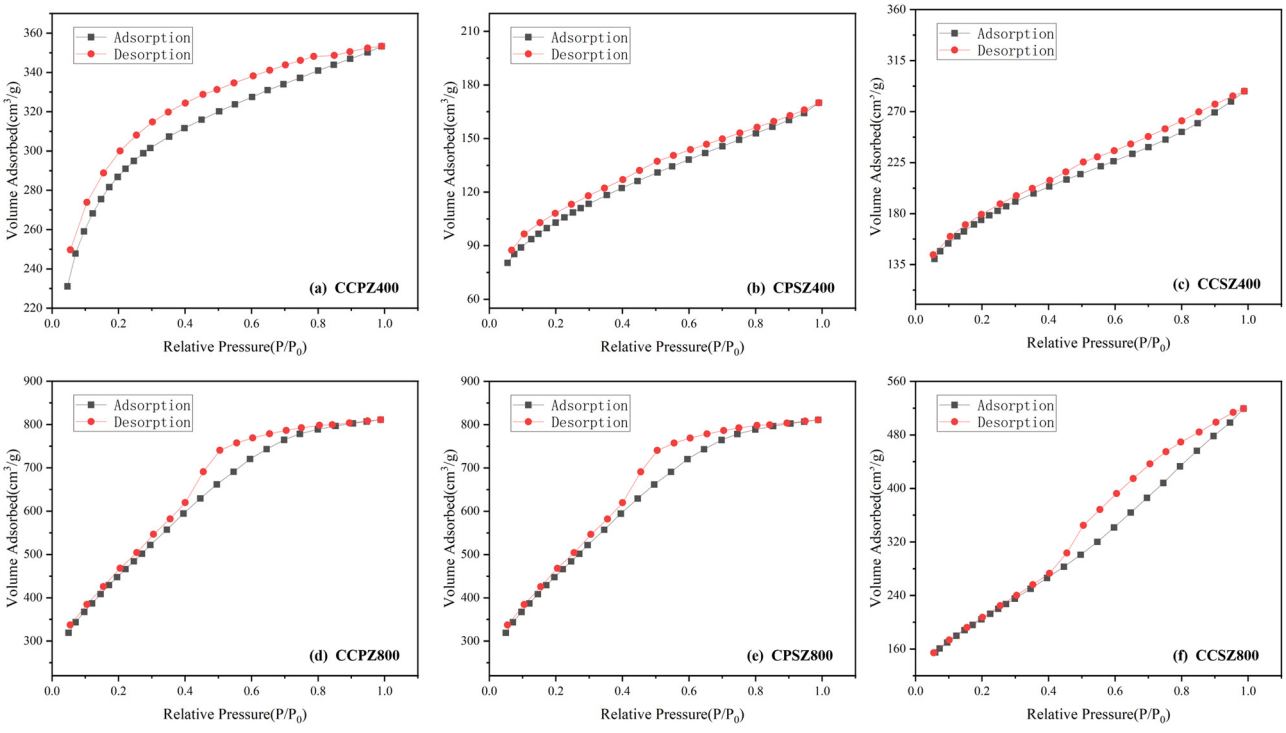

Figure 2: N_2 adsorption/desorption diagram of modified porous carbon. (a) CCPZ400, (b) CPSZ400, (c) CCSZ400, (d) CCPZ800, (e) CPSZ800, and (f) CCSZ800.

3.2 Characterization of the chemical structure of carbon materials

FTIR analysis revealed that both the raw and unmodified carbon materials (Figure 3a–c) exhibited stretching vibrations of –OH (3,400–3,650 cm^{-1}), (2,978–2,932 cm^{-1}), ester group C–O (1,045–1,100 cm^{-1}), and –C═O double bonds (1,670–1,715 cm^{-1}). The increase in temperature and the modification process resulted in the detachment of binding water in biomass, leading to the breakage of hydroxyl groups and an increase in hydrophobicity [22]. Consequently, the intensity of the –OH group peaks on the surface of the modified porous carbon (Figure 3d–f) gradually weakened or almost disappeared. Simultaneously, the stretching vibration of –COOH appeared on the surface (1,220 cm^{-1}), along with the stretching vibration of C═C double bond (1,540–1,640 cm^{-1}) and the bending vibration of aromatic hydrocarbon –CH (810–820 cm^{-1}). These changes were attributed to the continuous weakening of –CH2, resulting in the formation of an aromatic structure [23]. Additionally, in the fingerprint region below 600 cm^{-1}, a peak at 463 cm^{-1} (Figure 3e) was observed, indicating the stretching vibration of Zn–O. This peak may be attributed to the generation of Zn-containing oxides during the modification process.

XRD analysis revealed diffraction peaks at 2θ = 15°, 17°, and 22° for CP (Figure 4a), corresponding to the (1-10), (110), and (200) crystal planes of CE CE-I, which aligns with the standard CE crystal structure. Similarly, CS (Figure 4c) also exhibited a peak at 2θ = 22°. PS (Figure 4b) displayed peaks at 2θ = 29.1°, 30.9°, 40.9°, 44.9°, and 51.2°, corresponding to $CaMg(CO_3)_2$ (PDF No. 75-1655 and PDF No. 79-1342), respectively. Additionally, the SiO_2 peak (PDF No. 85-0539) was observed in both CS and PS, indicating the absorption of silicon elements from raw materials [24]. The high temperature and modification processes led to the disruption of the biomass's original structure, accelerated CE dissolution, and consequent weakening of the characteristic CE peaks in CP and CS. The SiO_2 diffraction peaks in PS were significantly attenuated after warming carbonization and modification, while the appearance of diffraction peaks corresponding to $CaSiO_3$ and Mg_2SiO_4 (PDF No. 77-5177 and PDF No. 74-1680) suggests the reaction of SiO2 with $CaMg(CO_3)_2$ at elevated pyrolysis temperatures, forming silicate. Moreover, CPSZ400/800 exhibited new diffraction peaks at 2θ = 36.3°, 42.1°, and 61.1°, corresponding to (111), (200), and (220) crystal plane reflections of ZnO (PDF No. 77-0191). The presence of Zn-O bonds on the surface of CPSZ400/800 is consistent with the FTIR results. CPSZ800 contains a small amount of elemental Zn on its surface, while no characteristic peaks of Zn were found on the surfaces of CCPZ800 and CCSZ800, which may cause less secondary contamination of elemental Zn in wastewater treatment.

Modified porous carbon materials exhibit a strong broad peak at 2θ = 25°, which is attributed to the carbon (002) crystal diffraction peak. This peak reflects the level of

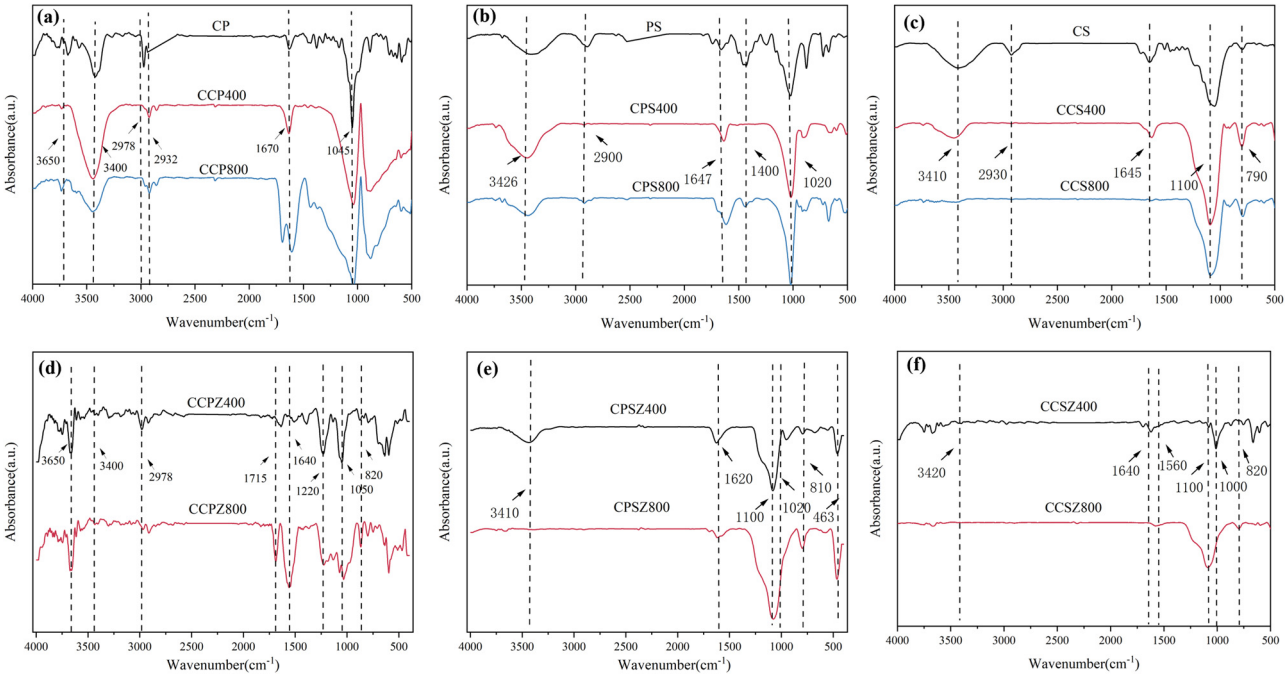

Figure 3: FTIR diagram of carbon material. (a–c) Three feedstocks and unmodified carbon materials and (d–f) Modified porous carbon from three raw materials.

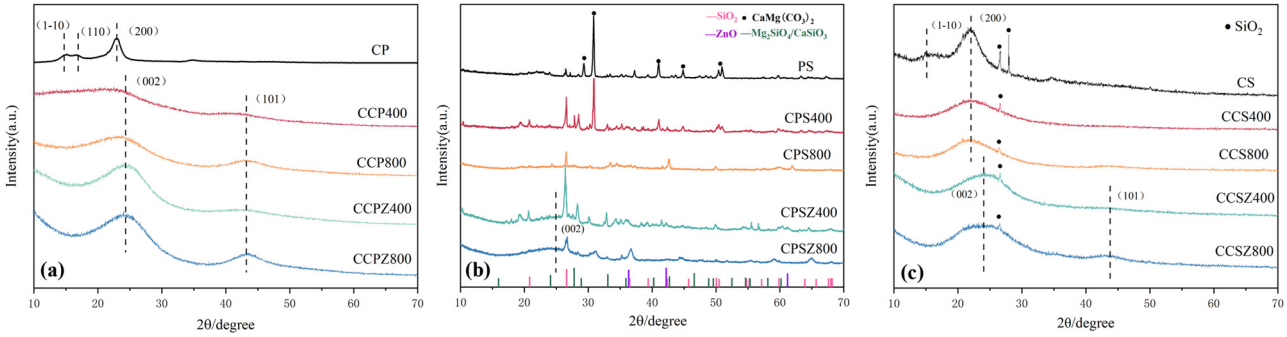

Figure 4: XRD diagram of carbon material. (a) Cotton pulp and its modified and unmodified carbon materials, (b) Poplar sawdust and its modified and unmodified carbon materials and (c) Corn stoever and its modified and unmodified carbon materials.

spatial order of the aromatic carbon lamellae. The peak symmetry and absence of nearby spurious peaks indicate that these carbon materials are composed of ordered and oriented polycyclic aromatic carbon lamellae [25]. Notably, CPSZ400 shows more γ-peaks, which are caused by the presence of aliphatic hydrocarbon chains connected to the edges of the aromatic carbon lamellae. Higher levels of LI in PS are more difficult to break down at low temperatures, as the temperature increases, the pyrolytic fracture of aromatic hydrocarbon side chains leads to a reduction in *γ*-peaks, resulting in a more regular and orderly structure in CPSZ800 [26]. Additionally, the broader peaks observed at $2\theta = 45°$ in both CP- and CS-modified porous carbons can be attributed to the carbon (101) crystal plane diffraction peaks. The sharper peaks observed in CPSZ800 and CCSZ800 indicate a higher degree of graphitization in these materials [27].

The XPS gross spectra (Figure 5a–c) indicate that all three types of modified porous carbon have high carbon content, with CCPZ800 having the highest carbon content. Additionally, CPSZ800 and CCSZ800 contain a small amount of Si, which is consistent with previous findings. The C1s split-peak fitted spectra (Figure 5d–f) of CCPZ800 reveal the highest C–C/C=C content, followed by CCPZ800 and CCSZ800. It is important to note that a shake-up peak of C1s appears at 291.18 eV next to the main peak of the C1s split-peak map of

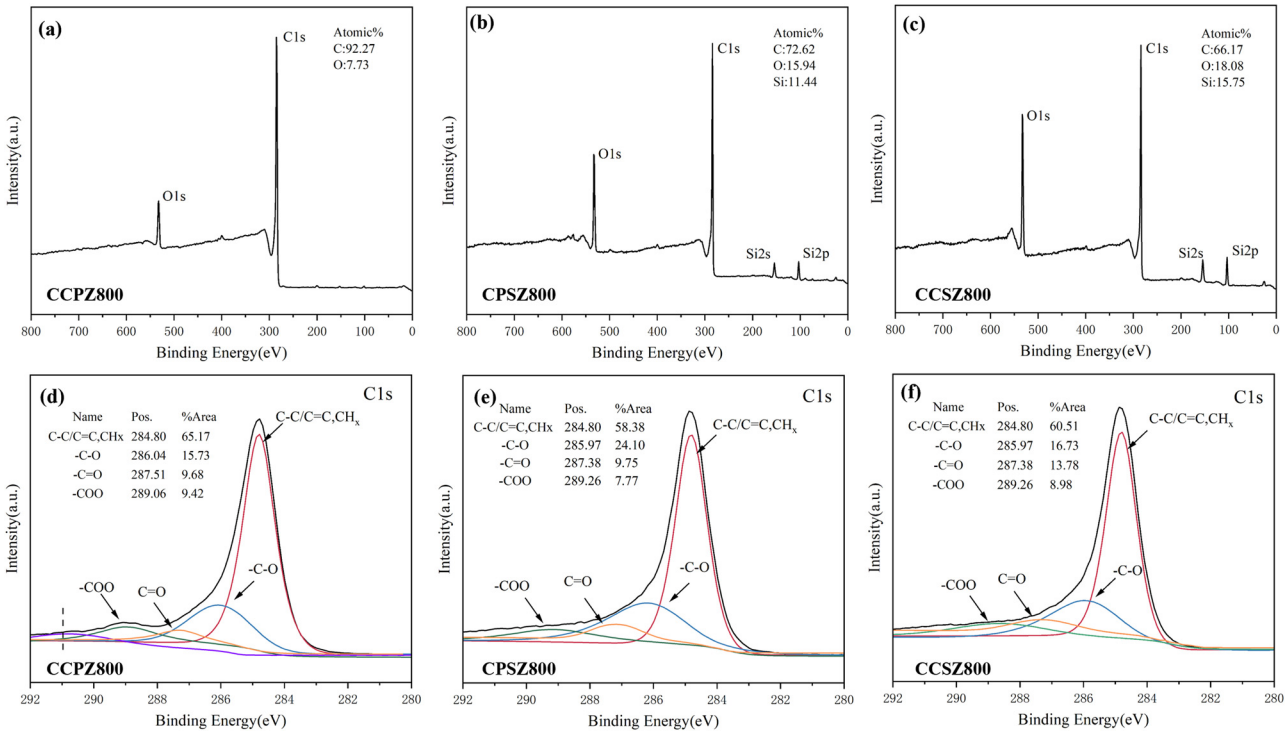

Figure 5: XPS diagram of carbon material. (a–c) XPS total mapping of porous carbon modified with three different raw materials and (d–f) C1s spectral profiles of porous carbon modified with three different raw materials.

Table 2: Adsorption of SDZ by carbon materials with different preparation conditions

Biomass	Temperature (°C)	Unmodified Q_e (mg/g)	Modified Q_e (mg/g)
CP	400	5.03	279.26
	800	19.77	425.45
PS	400	7.52	52.76
	800	23.67	214.99
CS	400	13.50	77.87
	800	25.12	130.10

CCPZ800 (Figure 5d). This peak is primarily caused by the presence of a π–π conjugation system [28]. The existence of conjugated π-bonds in the plane of C atoms leads to the appearance of a companion peak at a higher energy level. This indicates the strong π-electron supplying ability of CCPZ800. Moreover, the companion peak is also a characteristic peak of graphite π-bonding, suggesting that CCPZ800 contains a higher degree of graphite structure and a higher density of π-electrons on its surface [29]. Meanwhile, no significant amount of zinc was detected in the XPS spectra of the three modified porous carbons, suggesting that the material poses a low risk of zinc contamination of wastewater.

3.3 Adsorption experiment

Carbon materials with different preparation conditions were selected for the batch adsorption of SDZ to initially investigate the adsorption effect on SDZ (Table 2), and materials with excellent adsorption effects were preferred from each carbon source for the subsequent tests. CCPZ800, CPSZ800, and CCSZ800 were selected to investigate the adsorption of SDZ on modified porous carbon by changing the adsorption conditions.

The three modified porous carbon materials showed the maximum adsorption of SDZ at an additional amount of 1 mg (Figure 6a), which could reach 454.99, 239.50, and

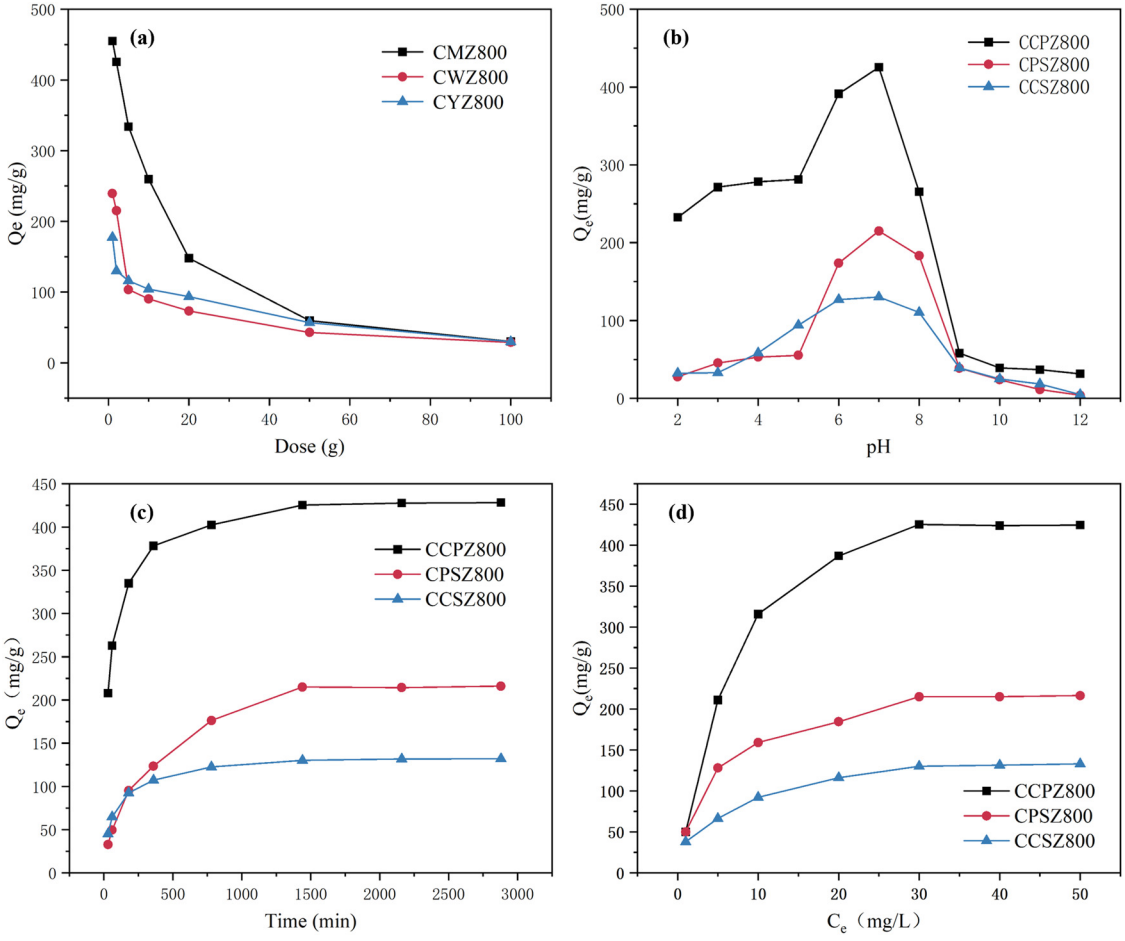

Figure 6: Effect of different conditions on the adsorption of modified porous carbon on SDZ. (a) Dose, (b) pH, (c) time, and (d) concentration.

177.27 mg/g, respectively, and the Q_e decreased with the increase in the addition amount. This is because the total adsorption capacity increases with the increase in the additional amount, but the amount of the target pollutant is certain, which leads to a decrease in the adsorption capacity per unit mass.

The adsorption amounts of the three modified porous carbons showed a tendency to increase and then decrease with the increase in pH (Figure 6b). Among them, CCPZ800, CPSZ800, and CCSZ800 all had the largest adsorption amounts at pH = 7, which could reach 425.45, 214.99, and 130.10 mg/g. Changes in acid and alkaline environments can affect the adsorption of SDZ, especially alkaline conditions have the most pronounced effect on SDZ adsorption.

SDZ are ionizable compounds and will exist as cations (SDZ^+), anions (SDZ^-), and neutral molecules (SDZ^0) in different pH backgrounds [30]. Since the zero point charge of pH (pH_{zpc}) of the three modified porous carbons ranges from 5.9 to 6.8 (Table 3), the modified porous carbons are electrostatically repelled from SDZ under acidic conditions (positive repulsion) and alkaline conditions (negative repulsion), thus inhibiting the adsorption [31]. This suggests that electrostatic action was not the primary adsorption mechanism for SDZ, which is consistent with the findings of Tzeng et al. [32].

SDZ is an aromatic compound that contains an aromatic heterocyclic ring. The amino and sulfonamide groups on SDZ^0 act as strong π-electron acceptors, while the modified porous carbon with aromaticity acts as a strong π-electron donor. The high temperature and modification effects increase the graphitization and hydrophobicity of the material, which results in a higher π-electron density on the surface of the modified porous carbon, which will facilitate the formation of π–π conjugation and thus enhancement of adsorption between the modified porous carbon and SDZ [33]. Acidic and basic conditions lead to a decrease in the π-electron density of SDZ, which can lead to a decrease in the π-electronic properties on the aromatic ring of SDZ, weakening the π–π conjugation with the modified porous carbon, and consequently decreasing the amount of adsorption [31].

In addition, SDZ^0 has hydrophobicity, and the modified porous carbon made by high-temperature pyrolytic carbonization has weakened hydrophilicity due to the enhancement of aromaticity, which also suggests that hydrophobicity distribution plays a role in the adsorption of SDZ on the modified porous carbon [34].

Table 3: Modified porous carbon for pH_{zpc}

Material	pH_{zpc}
CCPZ800	6.8
CPSZ800	5.9
CCSZ800	6.4

The adsorption equilibrium time of the three modified porous carbons on SDZ was about 1,440 min (Figure 6c), and the adsorption amount of SDZ increased rapidly in 0–600 min, and the increase in the adsorption amount slowed down in 600–720 min, and then gradually leveled off in 1,440 min. At the beginning of the reaction, the SDZ concentration was larger, the modified porous carbon possessed more effective adsorption sites, and SDZ would rapidly occupy multiple adsorption sites, resulting in an accelerated adsorption rate. With the decrease in effective adsorption sites, the adsorption rate decreased, the adsorption of SDZ was close to saturation, and the adsorption system reached equilibrium.

At low concentrations (1–30 mg/L), the adsorption of SDZ by the three modified porous carbons gradually increased with the increase in SDZ concentration (Figure 6c), but the adsorption of SDZ by the three modified porous carbons gradually stabilized when the concentration gradually reached 30 mg/L. At low concentrations of SDZ, SDZ could not completely occupy the adsorption sites of porous carbon during the adsorption process. As the concentration increases, the adsorption sites are gradually occupied, resulting in saturation adsorption due to the insufficiency of adsorption sites, and the adsorption amount tends to stabilize gradually [35].

3.4 Kinetics and isothermal adsorption

To further analyze the interaction between adsorbent and SDZ, it is important to analyze the adsorption kinetics and isothermal adsorption. The adsorption process of SDZ on modified porous carbon with quasi-primary, quasi-secondary kinetics fitting results (Figure 7) showed that the quasi-secondary kinetics R^2 = 0.9807, 0.9882, and 0.9935 for CCPZ800 (Figure 7a), CPSZ800 (Figure 7b), and CCSZ800 (Figure 7c) were greater than the quasi-primary kinetics of R^2 = 0.8658, 0.9753, 0.9894 (Table 4). And the quasi-secondary kinetic Q_e (CCPZ800 = 426.63 mg/g, CPSZ800 = 242.64 mg/g, CCSZ800 = 134.25 mg/g) was closer to the experimental values (CCPZ800 = 425.45 mg/g, CPSZ800 = 214.99 mg/g, CCSZ800 = 130.10 mg/g), which indicates that the quasi-secondary model is more consistent with the adsorption process of SDZ by these three modified porous carbons than the quasi-primary model. The quasi-primary kinetic model is commonly used to describe the initial stage of adsorption, specifically focusing on single-layer physical adsorption, It is obtained by parametric integration of the

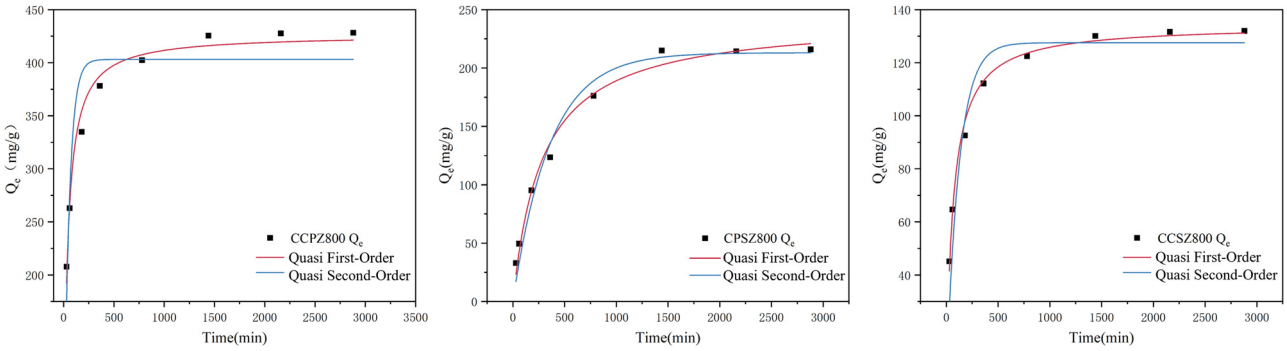

Figure 7: Kinetic fitting of SDZ adsorption by modified porous carbon.

Table 4: Adsorption kinetics fitting parameters

Model parameter		CCPZ800	CPSZ800	CCSZ800
Quasi-primary kinetic model	K_1	0.0190	0.0028	0.0001
	Q_e (mg/g)	403.0871	213.0637	133.6503
	R^2	0.8658	0.9753	0.9894
Quasi-secondary kinetic model	K_2	0.0006	0.0001	0.0001
	Q_e (mg/g)	426.6309	242.6377	134.2449
	R^2	0.9807	0.9882	0.9935

Lagergren equation, which has some limitations in practical applications. On the other hand, the quasi-secondary adsorption kinetic equation is mainly based on chemisorption, describes the whole process of adsorption, and contains multilayer adsorption with the joint action of various mechanisms (surface adsorption, intra-particle diffusion, etc.).

At the same time, the quasi-secondary adsorption kinetic model suggests that chemisorption may be an important factor in the whole adsorption process, and the adsorption process may be controlled by the interactions generated by adsorbent and adsorbate as well as by the exchange of electrons [36]. Therefore, the quasi-secondary kinetic equations of the three adsorbents were highly fitted, and the adsorption of SDZ on the three modified porous carbons could be preliminarily judged to be the result of multiple adsorption mechanisms, including chemisorption or physicochemical adsorption.

The isothermal adsorption model can well describe the distribution of adsorbent in the solid–liquid phase at adsorption equilibrium, and then explain the adsorption mechanism. The adsorption of SDZ by CCPZ800 (Figure 8a), CPSZ800 (Figure 8b), and CCSZ800 (Figure 8c) showed good linear relationships with the fits of both Langmuir isothermal adsorption model and Freundlich isothermal adsorption model, but the correlation coefficients of Freundlich isothermal adsorption model R^2 (CCPZ800 = 0.9815, CPSZ800 = 0.9639, and CCSZ800 = 0.9753) were higher than the correlation coefficients R^2 of the Langmuir isothermal adsorption model (CCPZ800 = 0.9684, CPSZ800 = 0.8966, and CCSZ800 = 0.8864) (Table 5), and the adsorption of SDZ on the three kinds of modified porous carbons by the Freundlich isothermal adsorption model showed good linear relationships.

The Langmuir isothermal adsorption model assumes the presence of numerous adsorption active sites on the surface of the adsorbent. Saturation adsorption is achieved when all the active sites are occupied. This model primarily

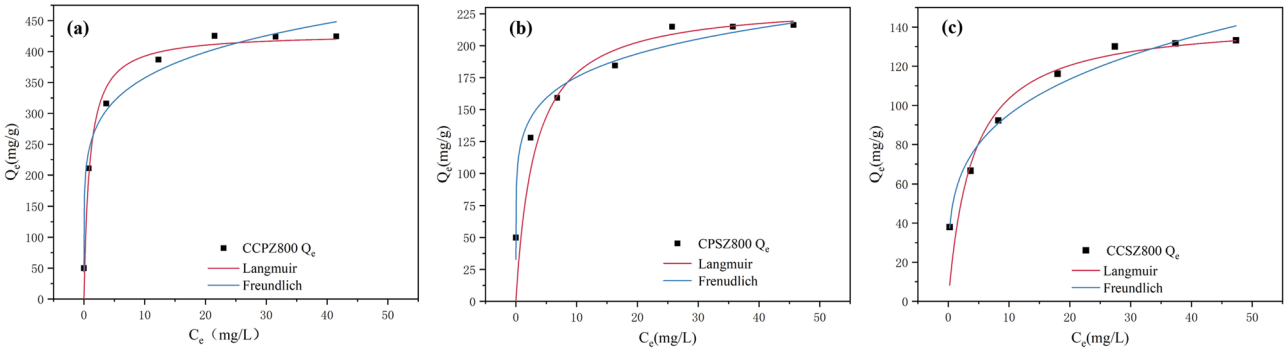

Figure 8: Isothermal adsorption fitting of modified porous carbon for SDZ adsorption. (a) CCPZ800 Q_e, (b) CPSZ800 Q_e, and (c) CCSZ800 Q_e.

Table 5: Isothermal adsorption fitting parameters

Model parameter		CCPZ800	CPSZ800	CCSZ800
Langmuir	K_L	1.0559	0.3199	0.2543
	Q_{max} (mg/g)	429.7380	234.3726	144.0729
	R^2	0.9684	0.8966	0.8864
Freundlich	K_F	247.4364	126.3029	53.5503
	n	6.2710	7.0048	3.9957
	R^2	0.9815	0.9639	0.9753

describes monomolecular layer adsorption. On the other hand, the Freundlich isothermal adsorption model assumes that the adsorption process takes place on a surface that is not uniform [37]. The amount of adsorption increases as the concentration of the target pollutant increases. This model mainly describes multimolecular layer adsorption. This is supported by the adsorption constants (n) in the Freundlich isothermal adsorption model, which are greater than 1 for all three modified porous carbons. The higher values of n suggest a stronger force between the modified porous carbons and SDZ, making the adsorption process easier to occur. This type of adsorption is known as favorable adsorption, adsorption of SDZ by modified porous carbon is a multimolecular layer adsorption and is a chemisorption-dominated adsorption mechanism [38].

Table 5 shows that the saturated adsorption Q_{max} of the three modified porous carbons were CCPZ800 = 429.7380 mg/g > CPSZ800 = 234.3726 mg/g > CCSZ800 = 144.0729 mg/g. Compared to other similar adsorbents in the literature (Table 6), CCPZ800 showed better adsorption capacity for SDZ removal.

3.5 Hydrothermal carbon and raw material composition adsorption experiment

The modified porous carbon is expected to have oxygen-containing functional groups that can form hydrogen bonding interactions with the amino groups of SDZ, it is possible that hydrogen bonding is also one of the main adsorption mechanisms Hydrothermal carbonization is a process that converts biomass into carbon nanomaterials in an aqueous phase, using specific temperature and pressure conditions [42]. The resulting hydrothermal carbon nanomaterials possess a significant amount of oxygen-containing functional groups on their surface. These functional groups can form hydrogen bonds with polar groups, such as amino groups, present on the surface of SDZ and enhance the adsorption effect on SDZ [43]. The adsorption Q_e of SDZ by the hydrothermal carbon materials HCCP, HCPS, and HCCS prepared by hydrothermal synthesis of the three raw materials were 25.37, 18.17, and 16.48 mg/g, respectively (Table 7). The adsorption capacity of the hydrothermal carbon material was significantly lower than that of the modified porous carbon. The limited adsorption of SDZ by the hydrothermal carbon material, which was enriched with oxygen-containing functional groups, suggests that the hydrogen-bonding effect produced by these groups on SDZ is not the primary adsorption mechanism.

There were differences in the adsorption capacity of the modified porous carbon from different carbon sources, and the distribution of the major constituents of the carbon source biomass might also affect the adsorption effect.

CE, HE, and LI are the primary constituents of biomass, along with a few other organic compounds and inorganic elements [44]. CE acts as the “skeleton,” HE functions as the “filler,” and LI acts as the “binder,” collectively forming a comprehensive biomass [45]. CP contains the highest amount of CE (>90%), PS contains more LI, and CS contains more HE than the other raw materials [46]. Modified porous carbon was prepared using CE, HE, and LI as carbon sources (same method as in 2.1 of this article) CCEZ400/800, CHEZ400/800, and CLIZ400/800, (400/800 stands for carbonization temperature), and SDZ was adsorbed to further investigate the effect of carbon source composition on adsorption.

Table 8 shows that the CE-modified porous carbon prepared at 800°C showed the highest adsorption, followed by LI and HE-modified porous carbon with 307.97, 256.33, and 156.83 mg/g, respectively. The variability in adsorption is due to the different behaviors of the constituent components during pyrolysis. CE in the lower temperature (<400°C) under the partial decomposition of CO_2, CO, H_2O, and other forms of release and produce coke and small molecules

Table 6: Table of saturation adsorption of SDZ by various adsorbents

Absorbent	Q_{max} (mg/g)	References
CCPZ800	429.74	This study
CPSZ800	234.37	
CCSZ800	144.07	
Ni/CNF	103.21	[39]
A 1/5 C800	261.00	[40]
BC900	206.03	[35]
MrGO-3	6.26	[41]

Table 7: Adsorption of SDZ by hydrothermal carbon

Hydrothermal carbon	Q_e (mg/g)
HCCP	25.37
HCPS	18.17
HCCS	16.48

Table 8: Adsorption of SDZ by modified porous carbon prepared from raw material components

Material	Temperature (°C)	Q_e (mg/g)
CCEZ400	400	94.74
CCEZ800	800	307.97
CHEZ400	400	49.45
CHEZ800	800	156.80
CLIZ400	400	17.53
CLIZ800	800	256.33

(hydroxyacetone, monosaccharides, etc.) and the formation of a certain pore structure, with the increase in temperature, while at high temperatures (>650°C), the small molecules through the decarbonylation and arylation of a large number of aromatic hydrocarbons, coke will be arylated into an aryl ring, and a large number of mesopores will be generated. The pyrolysis process of HE is similar to that of CE. It produces a significant amount of light-oxygenated compounds (such as acetic acid, propionic acid, and other compounds), coke, and a small amount of pore structure at temperatures below 400°C. At temperatures above 650°C, the coke undergoes further polymerization to form an aromatic ring [47]. Additionally, the oxygenated compounds undergo arylation, resulting in the generation of aromatic hydrocarbons along with some CO and H_2. This process also leads to the formation of mesoporous structure. In contrast, LI is structurally more stable than CE because of its numerous aromatic rings. It primarily undergoes dehydration and softening reactions at low temperatures (<400°C), resulting in the production of intermediate products and a poor pore structure [48]. However, at higher temperatures (>650°C), the LI β–O-4 linkage breaks down, leading to the formation of carbon nanosheets within the aromatic units. Additionally, the coke produced by LI enhances its aromaticity through the arylation reaction, resulting in the generation of a larger number of micropores [49]. The pyrolysis products of CE, HE, and LI produced at higher carbonization temperatures exhibit greater aromaticity compared to those produced at lower temperatures. This increased aromaticity enhances the adsorption of SDZs through π–π conjugation. Therefore, modified porous carbon materials carbonized at 800°C demonstrate a superior adsorption.

Due to its lower degree of polymerization compared to CE, HE is more easily decomposed [50]. At high temperatures, HE undergoes almost complete decomposition, resulting in a weaker aromaticity in the CE product. This weaker aromaticity can potentially reduce the adsorption of SDZ. This explains the difference in SDZ adsorption by CCPZ/CCEZ and CCSZ/CHEZ [51].

The modifier and high-temperature effects can disrupt the graphitic structure of CE-derived carbon. This disruption is beneficial as it increases the graphitization of the carbon. Higher graphitization, in turn, results in a higher π-electron density on the surface of the carbon. This higher π-electron density potentially promotes the π–π conjugation of modified porous carbon to SDZ, enhancing the adsorption effect [52]. It is possible that this is the reason why CCPZ presents better adsorption properties to SDZ [53].

The distribution of biomass raw materials and the pyrolysis temperatures have different effects on the adsorption of SDZ by the pyrolysis products of porous carbon. Under lower temperature preparation conditions, the adsorption effects of the modified pyrolysis products' three components on SDZ were as follows: CE > HE > LI. However, under higher temperature preparation conditions, the adsorption effects of the three components on SDZ were: CE > LI > HE. The adsorption effect of the modified pyrolysis products' three components on SDZ was found to be highest at higher temperature preparation conditions, with CE having the strongest effect. Therefore, when selecting a carbon source for the preparation of porous carbon for SDZ adsorption, biomass with higher CE content should be chosen. Additionally, if the carbon source biomass has a higher LI content, it should be subjected to elevated carbonization temperature to improve the experimental outcome.

4 Conclusion

The modified porous carbon was prepared using $ZnCl_2$ as a modifier and different carbon sources were selected at varying temperatures through the oxygen-limited cracking method. The physical and chemical properties of the carbon were characterized, and its adsorption performance was investigated using SDZ as the target pollutant. The aim of this study was to explain the adsorption mechanism and the reasons for the variability in adsorption among different carbon sources. The results of the study are as follows:

High temperature and modification can lead to the destruction of the original morphology of feedstock biomass, resulting in significant changes and reorganization of its microstructure. This process also leads to the formation of a pore structure in the modified porous carbon, which has a large specific surface area and pore volume. The modified porous carbon prepared at the higher carbonization temperature (800°C) was dominated by mesoporous structure, while the modified porous carbon prepared at the lower carbonization temperature (400°C) was dominated by microporous structure. High temperatures

and modifications help to increase the functional group structure of the porous carbon surface and enhance the aromaticity and graphitization of the porous carbon. Among the modified porous carbons prepared at 800°C, CCPZ800 has the highest degree of carbonization and graphitization, indicating a higher carbon content and its adsorption of SDZ was the largest, reaching 425.45 mg/g, followed by CPSZ800 and CCSZ800. The results showed that higher carbonization temperature and the modification effect of $ZnCl_2$ could enhance the adsorption of SDZ on porous carbon.

CCPZ800, CPSZ800, and CCSZ800 exhibited the highest adsorption capacity for SDZ at pH = 7. The adsorption equilibrium time was approximately 1,440 min, and the adsorption process followed the quasi-secondary adsorption kinetic model and Freundlich isothermal adsorption model. The saturated adsorption amounts were as follows: CCPZ800 (429.74 mg/g) > CPSZ800 (234.37 mg/g) > CCSZ800 (144.07 mg/g). The Q_{max} of CCPZ800 for SDZ is slightly better than other adsorbent materials prepared in the literature. The poor adsorption of SDZ on hydrothermal carbon materials enriched with oxygen-containing functional groups suggests that hydrogen bonding of SDZ by oxygen-containing functional groups on the surface is not the main adsorption mechanism. The variation in the distribution of carbon source biomass components resulted in differences in pyrolysis products, thereby impacting the adsorption process. Specifically, a higher biomass CE content led to improved adsorption efficiency of SDZ by the modified porous carbon material. The stronger aromaticity, higher degree of carbonization and graphitization of modified porous carbon enhance the π–π conjugation and thus the adsorption of sulphadiazine, which may be the reason for the differences in the adsorption of sulphadiazine by modified porous carbon prepared from different raw materials and methods.

The adsorption mechanism of SDZ on $ZnCl_2$-modified porous carbon was chemisorption-dominated multimolecular layer adsorption, it contains a cooperative interaction of physical pore adsorption, electrostatic attraction, hydrogen bonding, and π–π conjugation, and π–π conjugation played the most significant role. Additionally, hydrophobicity partitioning also contributed to the adsorption process.

5 Limitations and future research

In this study, $ZnCl_2$-modified porous carbon was successfully prepared using different raw materials and modification conditions, and its physical and chemical property characteristics were investigated to study the adsorption effect and mechanism of SDZ in the aqueous environment, and to explore the effects of different carbon sources and preparation conditions on the adsorption effect, which provides theoretical and technological help to carry out the remediation work of SDZ pollution.

However, there are parts of this study that need to be improved and thought deeply, based on which this study still needs to improve and explore the experiments and contents for the following elements to make the results more perfect and scientific.

In this study, SDZ was selected as a single target pollutant, but wastewater often contains a variety of pollutants, so it is necessary to conduct adsorption experiments when a variety of common pollutants are mixed in subsequent experiments, and to examine the selective adsorption and competitive adsorption by modified porous carbon.

Alternatively, in the actual treatment of contaminated wastewater by adsorbent materials, it is particularly important to prevent secondary pollution, which will directly affect the effect of adsorbent materials to treat wastewater, in the subsequent experiments should be optimized preparation process, as far as possible to reduce the modifiers and other exogenous substances on the water environment caused by secondary pollution.

The long-term stability and regeneration of the adsorbent material is particularly important, and subsequent experiments are needed to demonstrate how the modified porous carbon behaves over multiple use cycles and whether the adsorption capacity changes over time, loaded with magnetic material to facilitate separation from the water column, which will be beneficial in demonstrating the value of the material for practical applications.

The preparation temperature of modified porous carbon in this experiment was only up to 800°C, the experimental results of this study show that a higher carbonization temperature can enhance the adsorption of SDZ on porous carbon, so a higher carbonization temperature (>900°C) can be chosen to investigate the adsorption performance of the pollutants in the subsequent experiments on the preparation of modified porous carbon.

This study mainly focuses on the adsorption of SDZ in the aqueous environment, while antibiotic contamination usually involves the water and soil environments, and the remediation of SDZ-contaminated soils can be considered in subsequent experiments by using this experimental material.

Funding information: This research was funded by Shaanxi Province Key Research Program Project (2023-ZDLSF-28) and Shaanxi Land Engineering Construction Group internal scientific research project (DJNY-YB-2023-27, DJNY2024-21, and DJNY-YB-2023-21).

Author contributions: Methodology: J.W. and L.Z.; software: T.C.; validation: H.Z. and Y.S.; formal analysis: Y.W. and C.Y.; data curation: Y.H.; writing – original draft: J.W.; writing – review and editing: L.Z. and T.C.; supervision: H.Z. and Y.S. All authors have read and agreed to the published version of the manuscript.

Conflict of interest: Authors J.W., L.Z., T.C., H.Z., Y.S., Y.W., C.Y., and Y.H. were employed by the company Shaanxi Provincial Land Engineering Construction Group Co., Ltd. The authors declare that the research was conducted in the absence of any commercial or financial relationships that could be construed as a potential conflict of interest.

Ethical approval: The conducted research is not related to either human or animal use.

Data availability statement: All data generated or analyzed during this study are included in this published article (and its supplementary information files).

References

[1] Ponka D. Approach to managing patients with sulfa allergy: Use of antibiotic and nonantibiotic sulfonamides. Can Fam Physician Med de Famille Canadien. 2006;52(11):1434–8.

[2] Guo X, Li J, Yang F, Yang J, Yin D. Prevalence of sulfonamide and tetracycline resistance genes in drinking water treatment plants in the Yangtze River Delta, China. Sci Total Environ. 2014 Sep;493:626–31.

[3] Fahad MM, Al-Khuzaie MGA. Recent advances in sulfadiazine's preparation, reactions and biological applications. Euras Chem Commun. 2021;3:383–91.

[4] Zhou H, Cui J, Li X, Wangjin Y, Pang L, Li M, et al. Antibiotic fate in an artificial-constructed urban river planted with the algae Microcystis aeruginosa and emergent hydrophyte. Water Environ Res. 2022;94(1):e1670.

[5] Ting-Ting Z, Zong-Cai TU, Ping-Ping T, Lu Z, Xiao-Mei S, Hui W. Histopathology of carassius auratus gibelio after sulfadiazine exposure in water environment. Acta Hydrobiol Sin. 2018;42:47–56.

[6] Wehrhan A, Streck T, Groeneweg J, Vereecken H, Kasteel R. Long-term sorption and desorption of sulfadiazine in soil: experiments and modeling. J Environ Qual. 2010;39(2):654–66.

[7] Zhang WW, Gong AJ, Lina Q, Cao YQ, Yuan XT. Processes of degradation and removal methods of antibiotics from waste water. Chin J Antibiot. 2013;38(9):401–10.

[8] Wang S, Gao B, Zimmerman AR, Li Y, Ma L, Harris WG, et al. Removal of arsenic by magnetic biochar prepared from pinewood and natural hematite. Bioresour Technol. 2015;175:391–5. doi: 10.1016/j.biortech.2014.10.104.

[9] Dong J, Li P, Ji X, Kang Y, Yuan X, Tang J, et al. Electrons of d-orbital (Mn) and p-orbital (N) enhance the photocatalytic degradation of antibiotics by biochar while maintaining biocompatibility: A combined chemical and biological analysis. J Hazard Mater. 2023Jun;451:131083.

[10] Zhu X, Li C, Li J, Xie B, Lü J, Li Y. Thermal treatment of biochar in the air/nitrogen atmosphere for developed mesoporosity and enhanced adsorption to tetracycline. Bioresour Technol. 2018;475–82.

[11] Munir R, Ali K, Naqvi SAZ, Muneer A, Bashir MZ, Maqsood MA, et al. Green metal oxides coated biochar nanocomposites preparation and its utilization in vertical flow constructed wetlands for reactive dye removal: Performance and kinetics studies. J Contam Hydrol. 2023 May;256:104167.

[12] He X, Ling P, Yu M, Wang X, Zheng M. Rice husk-derived porous carbons with high capacitance by $ZnCl_2$ activation for supercapacitors. Electrochim Acta. 2013;105(26):635–41.

[13] Ifi DZ, Aydn N. Comparison of H_3PO_4 and $ZnCl_2$ activated filtered coffee waste carbon-based adsorbents in methylene blue removal by using ultrasonic-assisted adsorption. Arab J Sci Eng. 2022;48(7):8641–53.

[14] Benmahdi F, Oulmi K, Khettaf S, Kolli M, Merdrignac-Conanec O, Mandin P. Synthesis and characterization of microporous granular activated carbon from Silver berry seeds using $ZnCl_2$ activation. Fuller Nanotube Carbon Nanostruct. 2021;9(29):657–69.

[15] Minaei S, Benis KZ, Mcphedran KN, Soltan J. Evaluation of a $ZnCl_2$-modified biochar derived from activated sludge biomass for adsorption of sulfamethoxazole. Chem Eng Res Des. 2023;190:407–20.

[16] Xia D, Tan F, Zhang C, Jiang X, Chen Z, Li H, et al. $ZnCl_2$-activated biochar from biogas residue facilitates aqueous As(III) removal. Appl Surf Sci. 2016;377:361–9.

[17] Sudhakar MP. Activation strategies for biochar to use as an efficient catalyst in various applications. Fuel. 2021;285:119205.

[18] Yu S, Zhou J, Ren Y. Excellent adsorptive-photocatalytic performance of zinc oxide and biomass derived N, O-contained biochar nanocomposites for dyes and antibiotic removal. Chem Eng J. 2022;451:138959.

[19] Zheng H, Wang Z, Zhao J, Herbert S, Xing B. Sorption of antibiotic sulfamethoxazole varies with biochars produced at different temperatures. Environ Pollut. 2013;181(1):60–7.

[20] Teixidó M, Pignatello JJ, Beltrán JL, Granados M, Peccia J. Speciation of the ionizable antibiotic sulfamethazine on black carbon (biochar). Environ Sci Technol. 2011;45(23):10020.

[21] Sing KSW, Williams RT. Physisorption hysteresis loops and the characterization of nanoporous materials. London, England: SAGE Publications; 2004. p. 773–82.

[22] Wang L, Wang X, Zou B, Ma X, Qu Y, Rong C, et al. Preparation of carbon black from rice husk by hydrolysis, carbonization and pyrolysis. Bioresour Technol. 2011;102(17):8220–4. doi: 10.1016/j.biortech.2011.05.079.

[23] Wang P, Tang L, Wei X, Zeng G, Zhou Y, Deng Y, et al. Synthesis and application of iron and zinc doped biochar for removal of p-nitrophenol in wastewater and assessment of the influence of co-existed Pb(II). Appl Surf Sci. 2017;392:391–401. doi: 10.1016/j.apsusc.2016.09.052.

[24] Wang Z, Yang X, Qin T, Liang G, Li Y, Xie X. Efficient removal of oxytetracycline from aqueous solution by a novel magnetic clay–biochar composite using natural attapulgite and cauliflower leaves. Environ Sci Pollut Res Int. 2019;26(8):7463–75. doi: 10.1007/s11356-019-04172-8.

[25] Wen Y, Tang X, Li J, Hao J, Wei L, Tang X. Impact of synthesis method on catalytic performance of MnO_x–SnO_2 for controlling formaldehyde emission. Catal Commun. 2009;10(8):1157–60.

[26] Sonibare OO, Haeger T, Foley SF. Structural characterization of Nigerian coals by X-ray diffraction, Raman and FTIR spectroscopy. Energy (Oxf). 2010;35(12):5347–53. doi: 10.1016/j.energy.2010.07.025.
[27] Huang Q, Chen H, Xu L, Lu D, Tang L, Jin L, et al. Visible-light-activated photoelectrochemical biosensor for the study of acetylcholinesterase inhibition induced by endogenous neurotoxins. Biosens Bioelectron. 2013;45:292–9. doi: 10.1016/j.bios.2013.01.075.
[28] Luo L, Shen X, Song L, Zhang Y, Zhu B, Liu J, et al. MoS_2/Bi_2S_3 heterojunctions-decorated carbon-fiber cloth as flexible and filter-membrane-shaped photocatalyst for the efficient degradation of flowing wastewater. J Alloy Compd. 2019;779:599–608. doi: 10.1016/j.jallcom.2018.11.154.
[29] Ji L, Chen W, Zheng S, Xu Z, Zhu D. Adsorption of sulfonamide antibiotics to multiwalled carbon nanotubes. Langmuir. 2009;25(19):11608–13. doi: 10.1021/la9015838.
[30] Ma D, Wang J, Feng K. A green strategy from waste red mud to Fe~0-based biochar for sulfadiazine treatment by peroxydisulfate activation. Chem Eng J. 2022;446:441P–6P.
[31] Xie M, Chen W, Xu Z, Zheng S, Zhu D. Adsorption of sulfonamides to demineralized pine wood biochars prepared under different thermochemical conditions. Environ Pollut. 2014;186:187–94.
[32] Tzeng T, Liu Y, Deng Y, Hsieh Y, Tan C, Wang S, et al. Removal of sulfamethazine antibiotics using cow manure-based carbon adsorbents. Int J Environ Sci Technol. 2016;13(3):973–84.
[33] Ahmad M, Lee SS, Dou X, Mohan D, Sung JK, Yang J, et al. Effects of pyrolysis temperature on soybean stover- and peanut shell-derived biochar properties and TCE adsorption in water. Bioresour Technol. 2012;118:536–44.
[34] Zhao H, Liu X, Cao Z, Zhan Y, Shi X, Yang Y, et al. Adsorption behavior and mechanism of chloramphenicols, sulfonamides, and non-antibiotic pharmaceuticals on multi-walled carbon nanotubes. J Hazard Mater. 2016;310:235–45. doi: 10.1016/j.jhazmat.2016.02.045.
[35] Zhang Z, Sun L, Pei Z, Li H, Wang L, Ma J, et al. New insight into the adsorption of sulfadiazine on graphite-like biochars prepared at different pyrolytic temperatures. J Clean Prod. 2023 Aug;413:137468.
[36] Nam S, Choi D, Kim S, Her N, Zoh K. Adsorption characteristics of selected hydrophilic and hydrophobic micropollutants in water using activated carbon. J Hazard Mater. 2014;270:144–52. doi: 10.1016/j.jhazmat.2014.01.037.
[37] Santos RKS, Nascimento BF, De ACMB, Cavalcanti JVFL, Bruckmann FS, Rhoden CRB, et al. Removal of chloroquine from the aqueous solution by adsorption onto acaí-based biochars: Kinetics, thermodynamics, and phytotoxicity. J Mol Liq. 2023;383:122162.
[38] Yang W, Lu Y, Zheng F, Xue X, Li N, Liu D. Adsorption behavior and mechanisms of norfloxacin onto porous resins and carbon nanotube. Chem Eng J. (Lausanne, Switzerland: 1996) 2012;179(1):112–8. doi: 10.1016/j.cej.2011.10.068.
[39] Xia S, Deng L, Liu X, Yang L, Pei Y. Fabrication of magnetic nickel incorporated carbon nanofibers for superfast adsorption of sulfadiazine: Performance and mechanisms exploration. J Hazard Mater. 2021;423(Pt B):127219.
[40] Li CXHY. Adsorption of two antibiotics on biochar prepared in air-containing atmosphere: Influence of biochar porosity and molecular size of antibiotics. J Mol Liq. 2019;274:353–61.
[41] Zhong J, Feng Y, Li JL, Yang B, Ying GG. Removal of sulfadiazine using 3D interconnected petal-like magnetic reduced graphene oxide (MrGO) nanocomposites. Water. 2020;12(7):1933.
[42] Zhurinsh A. Hydrothermal carbonization vs pyrolysis: effect on the porosity of the activated carbon materials. Sustainability. 2022;14:15982.
[43] Peng B, Liang S, Wang H, Meng Z, Guo M, Wang H, et al. In situ synthesis of low-valence MnO/Mn_3O_4 catalyst via carbon-acid hydrothermal strategy for NO removal. Mater Lett. 2022;327:133044.
[44] Kostryukov SG, Matyakubov HB, Masterova YY, Kozlov AS, Pryanichnikova MK, Pynenkov AA, et al. Determination of lignin, cellulose, and hemicellulose in plant materials by FTIR spectroscopy. J Anal Chem. 2023;78(6):718–27.
[45] Taherzadeh MJ, Karimi K. Pretreatment of lignocellulosic wastes to improve ethanol and biogas production: a review. Int J Mol Sci. 2008;9(9):1621–51. doi: 10.3390/ijms9091621.
[46] Díez D, Uruea A, Piero R, Barrio A, Tamminen T. Determination of hemicellulose, cellulose, and lignin content in different types of biomasses by thermogravimetric analysis and pseudocomponent kinetic model (TGA-PKM method). Processes. 2020;8(9):1048.
[47] Rojas M, Ruano D, Orrego-Restrepo E, Chejne F. Non-isothermal kinetics of cellulose, hemicellulose, and lignin degradation during cocoa bean shell pyrolysis. Biomass Bioenergy. 2023;177:106932.
[48] Ge L, Zhao C, Zuo M. Effects of Fe addition on pyrolysis characteristics of lignin, cellulose and hemicellulose. J Energy Inst. 2023;107:101177.
[49] Liu Z, Zhang F, Wu J. Characterization and application of chars produced from pinewood pyrolysis and hydrothermal treatment. Fuel (Guildf). 2010;89(2):510–4. doi: 10.1016/j.fuel.2009.08.042.
[50] Li C, Sun Y, Yi Z, Zhang L, Zhang S, Hu X. Co-pyrolysis of coke bottle wastes with cellulose, lignin and sawdust: Impacts of the mixed feedstock on char properties. Renewable Energy. 2022;181:1126–39.
[51] Xue P, Liu M, Yang H, Zhang H, Chen Y, Hu Q, et al. Mechanism study on pyrolysis interaction between cellulose, hemicellulose, and lignin based on photoionization time-of-flight mass spectrometer (PI-TOF-MS) analysis. Fuel. 2023;338:127276.
[52] Ma L, Syed-Hassan SSA, Tong Y. Interactions of cellulose-and lignin-derived radicals during pyrolysis: An in-situ electron paramagnetic resonance (EPR) study. Fuel Process Technol. 2023;239:107536.
[53] Deng J, Xiong T, Wang H, Zheng A, Wang Y. Effects of cellulose, hemicellulose, and lignin on the structure and morphology of porous carbons. ACS Sustainable Chem Eng. 2016;4(7):3750–6. doi: 10.1021/acssuschemeng.6b00388.